On the Variation of the Effective Breaking Strength in Oceanic Sea States[a]

CHRISTOPHER J. ZAPPA

Ocean and Climate Physics Division, Lamont-Doherty Earth Observatory, Columbia University, Palisades, New York

MICHAEL L. BANNER

School of Mathematics and Statistics, University of New South Wales, Sydney, New South Wales, Australia, and Ocean and Climate Physics Division, Lamont-Doherty Earth Observatory, Columbia University, Palisades, New York

RUSSEL P. MORISON

School of Mathematics and Statistics, University of New South Wales, Sydney, New South Wales, Australia

SOPHIA E. BRUMER

Ocean and Climate Physics Division, Lamont-Doherty Earth Observatory, Columbia University, Palisades, New York

(Manuscript received 21 November 2015, in final form 8 April 2016)

ABSTRACT

A spectral framework for quantifying the geometric/kinematic and dynamic/energetic properties of breaking ocean waves was proposed by Phillips in 1985. Phillips assumed a constant breaking strength coefficient to link the kinematic/geometric breaking crest properties to the associated excess energy and momentum fluxes from the waves to the upper ocean. However, a scale-dependent (spectral) breaking strength coefficient is needed, but is unavailable from measurements. In this paper, the feasibility of a parametric mean effective breaking strength coefficient valid for a wide range of sea states is investigated. All available ocean breaking wave datasets were analyzed and complemented with wave model behavior. Robust evidence is found supporting a single linear parameter relationship between the effective breaking strength and wave age or significant wave steepness. Envisaged applications for the effective breaking strength are described.

1. Introduction

Characterization of wave breaking on the sea surface provides a potentially valuable measure of the strength of air–sea interaction fluxes. The capability of imaging breaking waves from airborne (Kleiss and Melville 2010) and stable platforms (Gemmrich et al. 2008, 2013; Schwendeman et al. 2014; Sutherland and Melville 2013, 2015; Thomson et al. 2009; Zappa et al. 2012) provides exciting prospects for improved understanding and parameterization of several key air–sea interaction processes in the open ocean. These include momentum exchange associated with airflow separation (Mueller and Veron 2009a; Reul et al. 2008; Veron et al. 2007), sea spray generation (de Leeuw et al. 2011; Mueller and Veron 2009b), enhanced gas exchange (Asher and Wanninkhof 1998a,b; Keeling 1993; Merlivat and Mémery 1983; Woolf 1993, 2005), and near-surface and upper ocean optical variability (Dickey et al. 2011, 2012), among others. This capability also interfaces with developments utilizing satellite microwave remote sensing for various applications (Anguelova and Webster 2006; Hwang 2012; Hwang et al. 2008; Reul and Chapron 2003). There is also a pressing need for climate studies to include operational predictions using the wealth of available satellite data. Realizing this goal depends on optimally transforming data from both satellites and buoys into integrated breaking statistics, such as active whitecap fraction.

[a] Lamont-Doherty Earth Observatory Contribution Number 8018.

Corresponding author address: Christopher J. Zappa, Lamont-Doherty Earth Observatory, Columbia University, 61 Route 9W, Palisades, NY 10964.
E-mail: zappa@ldeo.columbia.edu

DOI: 10.1175/JPO-D-15-0227.1

a. *Phillips' (1985) spectral breaking wave framework*

Recent developments in the spectral characterization of breaking wave properties (Phillips 1985, hereinafter P85) in terms of the spectral density of breaking crest length per unit area $\Lambda(k)$ [or $\Lambda(c)$], and associated spectral breaking strength $b(k)$ [or $b(c)$], where k is wavenumber and c is phase speed, have added a new theoretical and observational framework that potentially adds reliable breaking wave information to routine wave forecasts (e.g., Banner and Morison 2010; Romero et al. 2012; Kukulka and Hara 2008a,b). With this increased measurement and modeling capability, it is timely to investigate further the quantification of the influence of breaking waves in air–sea interaction, especially its role in gas and sea spray exchange, by highlighting a potentially useful breaking strength parameter, b_{eff}, to be defined below.

In brief, the directional wave energy spectrum evolves according to the radiative transfer equation (Komen et al. 1994), shown below for deep water and negligible currents:

$$\frac{\partial \Phi}{\partial t} + \mathbf{c}_g \cdot \nabla \Phi = S_{\text{wave}}, \tag{1}$$

where $\Phi = \rho g \Psi(\mathbf{k})$ is the directional wave energy spectrum, $\int_0^\infty \Psi(\mathbf{k}) d\mathbf{k} = \overline{\eta^2}$ is the mean square wave height, $\mathbf{c}_g$ is the group velocity, ρ is the density of water, and g is the acceleration due to gravity. The total source term $S_{\text{wave}} = S_{\text{in}} + S_{\text{nl}} + S_{\text{ds}}$, where S_{in} is the atmospheric input spectral source term, S_{nl} is the nonlinear spectral transfer source term representing nonlinear wave–wave interactions, and S_{ds} is the spectral dissipation rate, assumed primarily due to wave breaking. Breaking wave dissipation rates have been shown to be roughly 5–1000 times greater than wall layer scaling (Agrawal et al. 1992; Gemmrich 2010; Sutherland and Melville 2015; Terray et al. 1996). In this context, Sutherland and Melville (2015) note that as the wave age increases, the total turbulent kinetic energy (TKE) dissipation rate within the wave boundary layer greatly exceeds the classical wall layer dissipation rate.

In view of the central role of surface and breaking waves in upper ocean dynamics and air–sea fluxes, wave and breaking measurements are paramount. The dissipation of wave energy in the energetic part of the spectrum has attracted considerable recent interest. Presently, parametric versions of S_{ds} based on satellite data are used in the context of active whitecap fraction (Anguelova and Hwang 2016), of ocean swell dissipation (Ardhuin et al. 2009), and of the TKE dissipation rate due to breaking (Hwang and Sletten 2008).

Underpinning the P85 breaking wave framework are the assumptions that 1) the velocity of a breaking front is equal to the phase velocity $\mathbf{c}$ of the underlying gravity wave that is breaking; 2) there is geometric self-similarity of the breaking zone (i.e., the cross-sectional area of the breaking region scales with c^4); and 3) the deep water dispersion formula relates the observed breaker front velocity to the underlying wavenumber $\mathbf{k}$ of the breaking wave. In this context, generic wave crest slowdown (Banner et al. 2014a) needs to be taken into account in transforming between the $\mathbf{c}$ and $\mathbf{k}$ domains. Published studies (e.g., Kleiss and Melville 2010; Gemmrich et al. 2013) indicate that Doppler correction by the orbital motion of long waves affecting the short waves produces only modest changes to breaking crest length per unit area $[\Lambda(\mathbf{c})]$ spectra, as defined in P85. We also note that the linear deep water gravity wave dispersion relation underpins Eq. (6.3) of P85, which was modified by Banner and Morison (2010) to establish the spectral form of the dissipation rate distribution associated with wave breaking, expressed in terms of the breaking wave phase velocity $\mathbf{c}$:

$$S_{\text{ds}}(\mathbf{c}) d\mathbf{c} = b(\mathbf{c}) \rho c^5 \Lambda(\mathbf{c}) d\mathbf{c}/g. \tag{2}$$

Note that S_{ds} is used here rather than ε as used in P85. Here, the nondimensional coefficient $b(\mathbf{c})$ is the scale-dependent breaking strength.

The directionally integrated form of Eq. (2) is

$$S_{\text{ds}}(c) dc = b(c) \rho c^5 \Lambda(c) dc/g, \tag{3}$$

which defines the turbulent energy dissipation rate $S_{\text{ds}}(c)$ due to active breaking at scale c and its relationship with $\Lambda(c)$ and $b(c)$. For narrow-banded wave systems typically used in laboratory dissipation rate determinations for breaking, b is assumed to be independent of scale and is found to be a strong function of the characteristic wave steepness (Banner and Peirson 2007; Drazen et al. 2008; Melville 1994). In ocean wave forecasting, spectral modeling studies provide evidence that $b(c)$ may scale with wave age (Banner and Morison 2010; Romero et al. 2012).

b. *The effective breaking strength*

The Phillips framework provides a compact parameterization for estimating the whitecap fraction, the momentum flux and the TKE dissipation rate from breaking waves. These quantities can be expressed as various moments of $\Lambda(c)$. Rather than working with the spectral breaking strength, $b(c)$, which is not presently known from measurements, we modify Eq. (3) by defining the effective breaking strength coefficient

$$b_{\text{eff}} = \int_c S_{\text{ds}}(c)\, dc \Big/ \left[\rho g^{-1} \int_c c^5 \Lambda(c)\, dc \right], \tag{4}$$

where $S_{ds}(c)$ also cannot yet be measured directly and presently has only been estimated from models (Morison and Banner 2016, manuscript submitted to *Ocean Modell.*; Romero et al. 2012). Furthermore, the integral of $S_{ds}(c)$ has been inferred from turbulence measurements in the wave boundary layer. The parameter b_{eff} is potentially very useful in a growing number of applications as described in section 4b below. The basis of the b_{eff} construct rests on the documented dominance of the breaking wave contribution to the TKE dissipation rate in the wave boundary layer (Agrawal et al. 1992; Gemmrich 2010; Sutherland and Melville 2015; Terray et al. 1996).

Following Gemmrich et al. (2013) among others (e.g., Schwendeman et al. 2014; Thomson et al. 2009), b_{eff} was quantified through the relation between the fifth moment of $\Lambda(c_b)$ and the depth-integrated, total energy dissipation rate, ε, in the wave boundary layer,

$$b_{eff} = \varepsilon \Big/ \left[\rho g^{-1} \int_c c_b^5 \Lambda(c_b)\, dc_b \right], \tag{5}$$

where c_b is defined as the "characteristic" speed of the breaker front (a turbulent layer flow) to distinguish it from the phase speed c of the underlying gravity wave that is breaking. The near-surface vertically integrated TKE dissipation rate, ε, may be decomposed into $\varepsilon = \varepsilon_{brk} + \varepsilon_{back}$, where ε_{brk} is due to wave breaking (whitecapping and microbreaking) and ε_{back} is the background TKE dissipation rate associated with wind shear and wave turbulence interaction among other processes (Sullivan and McWilliams 2010; Thais and Magnaudet 1996; Veron and Melville 2001). Note that ε is an independent measure of the mean depth-integrated dissipation rate in the wave boundary layer available from subsurface measurements or determined from modeling or parameterization.

As noted above, the background TKE dissipation rate is a small fraction of the total TKE dissipation rate in the presence of significant wave breaking. On this basis ε_{brk} dominates ε, and the TKE dissipation rate in the wave boundary includes some background turbulence as a residual. In this way, a reliable estimate for the total KE flux into the water column mediated by wave breaking can be obtained by combining b_{eff} with the fifth moment of $\Lambda(c_b)$.

In this note, we focus on the characterization of the effective breaking strength b_{eff}. We outline the historical laboratory measurements, field measurements, and modeling estimates for determining b_{eff}. We investigate the behavior of b_{eff} using field results and modeling estimates to determine the dominant dependence of b_{eff} with wave age, wave steepness, or wind speed. The sparse observational domain results for b_{eff} are complemented by modeling results to assess the likely general trend, which is subject to future validation. We develop a parameterization for b_{eff} as a function of wave age or significant wave steepness for use in operational forecasting. In the discussion section below (section 4), we highlight several geophysical products that would be enabled through the availability of a robust parameterization for b_{eff} that takes advantage of remotely sensed wave-field parameters to construct regional and global maps of these products.

2. Previous determinations of breaking strength

a. *Laboratory measurements*

Many measurements of laboratory narrow-banded unidirectional focused breaking wave systems have aimed to quantify the breaking strength in Eq. (4) above. The usefulness of these data has been to demonstrate dependences on wave properties (e.g., wave steepness) under controlled conditions, often without wind forcing (e.g., Banner and Peirson 2007; Drazen et al. 2008; Melville 1994; Perlin et al. 2013; Tian et al. 2010). However, it is a key open question as to whether this class of measurements is representative of breaking conditions in broad-banded directional sea states and hence it is not considered here.

b. *Field measurements*

Several measurement campaigns have aimed at determining b_{eff} in open ocean conditions. Phillips et al. (2001) measured "sea spikes" or discrete moving events in a set of X-band radar measurements, backscattered from the sea surface at near-grazing incidence with very high spatial and temporal resolution (30 cm in range and 2000-Hz pulse repetition frequency) in steady moderate wind speeds ($9.3 \pm 0.3\,m\,s^{-1}$) over the open ocean off Kauai, Hawaii. They measured $\Lambda(c_b)$ and inferred that b_{eff} according to equilibrium range wave theory spans the range (7–13) $\times 10^{-4}$ for a wave age, c_p/u_*, of 10, where c_p is the phase speed of the waves at the spectral peak and u_* is the atmospheric friction velocity. These authors stressed that their results provided no support for a "Kolmogorov cascade" in wind-generated waves analogous to that in turbulence (i.e., energy input from the wind to large wave scales and dissipation from the waves at small scales). The measurements indicate that, in contrast, dissipation is significant at the largest scales of wave breaking and is distributed widely across that spectrum. That is, there is no evidence that the wave energy dissipation is dominated by small-scale waves.

Thomson et al. (2009) analyzed video observations of breaking waves for wind speeds up to $15\,m\,s^{-1}$ taken from R/V *Henderson* at the north end of Lake

Washington in the state of Washington in 12-m water depth and on Puget Sound near Richmond Beach, Washington, in 19-m water depth. Energy dissipation by breaking water waves was quantified indirectly from video imagery using Fourier methods (Thomson and Jessup 2009) and directly from in situ acoustic Doppler velocity profile observations. Energy dissipation rate estimates are in reasonable agreement over two orders of magnitude when tuned by choosing $b_{\text{eff}} = 0.017 \pm 0.03$ (for direct measurements of dissipation) and $b_{\text{eff}} = 0.013 \pm 0.05$ (for indirect measurements of wind input). Peak waves were found to comprise only 10% of the total breaking rate, but they contributed up to 75% of the total dissipation rate. In addition, breaking statistics were found to depend on the peak wave steepness and the energy input by the wind.

Gemmrich et al. (2013) gathered open ocean video and dissipation rate observations from R/P *FLIP* in the Santa Barbara Channel (SBC) and in the Pacific Ocean (PO) off Hawaii during the Office of Naval Research (ONR)-sponsored Radiance in a Dynamic Ocean (RaDyO) experiments (Zappa et al. 2012). The Santa Barbara Channel observations had developing seas and the Pacific Ocean south of Hawaii had mature seas. During the PO experiment, the data show a distinctive and persistent decrease in the easterly wind speed from 10.2 m s^{-1} at the beginning of the experiment to 8.5 m s^{-1} at the end. The video data were analyzed to obtain breaking crest length distributions, $\Lambda(c_b)$, and the corresponding effective breaking strength during the wind-wave conditions. These are among the first experiments using dissipation rate measurements that probe up into the breaking crest regions, together with simultaneous measurements of breaking crest length distributions. The directly measured effective breaking strength parameter during the PO observations was $4.2\ (\pm 1.8) \times 10^{-5}$ in mature seas with wave age, c_p/u_*, of 40–47.

The integrated dissipation rate scaled by b_{eff} was consistently higher for mature seas compared to developing seas due to higher energy and momentum fluxes from the wind. In this note, we add the directly measured b_{eff} for the Santa Barbara Channel observations during RaDyO. The SBC experiment experienced a variety of conditions with generally low winds in the early morning with mean wind speed of 4.8 ± 2.7 m s^{-1} (all $\pm$ bounds refer to a combination of natural variability and measurement uncertainty as expressed by the standard deviation), and strong sea breezes up to 12 m s^{-1} in the evening with mean wind speeds of 7.1 ± 2.2 m s^{-1}. We determined b_{eff} to be $2.4\ (\pm 1.5) \times 10^{-3}$ in developing seas with wave age, c_p/u_*, of 22.3 ± 1.5. Here, the estimate of TKE dissipation rate was obtained at a depth of 0.75 m and following the methodology in Sutherland and Melville (2015) extrapolated to the surface based on z^{-1} scaling in order to determine ε.

Schwendeman et al. (2014) made coupled in situ and remotely sensed measurements of very strongly forced wind waves at short fetch to assess the role of breaking in a developing young wind sea in the Strait of Juan de Fuca, north of Sequim, Washington, aboard the R/V *Robertson* for wind speeds that ranged from 9.7 to 18.0 m s^{-1}. In situ measurements of TKE dissipation rate from wave-following SWIFT floats and a tethered acoustic Doppler sonar system are consistent with wave evolution and wind input estimated using the radiative transfer equation. The breaking crest length distribution $\Lambda(c_b)$ was obtained from stabilized shipboard video recordings and processed using the Fourier-based method of Thomson and Jessup (2009). The effective breaking strength parameter b_{eff} is calculated by comparing the fifth moment of $\Lambda(c_b)$ with the measured dissipation rates. The mean b_{eff} value was determined as 3.2×10^{-3}, with a standard deviation of 1.5×10^{-3}.

Sutherland and Melville (2015) investigated turbulent kinetic energy dissipation beneath breaking waves. Wind, wave, and turbulence measurements were made in the North Pacific Ocean aboard R/P *FLIP*, during the ONR-sponsored High Resolution Air–Sea Interaction (HiRes) and RaDyO experiments as well as off the Southern California coast (SoCal). SoCal 2010 took place over 2 days in the Southern California Bight in low to moderate wind conditions (up to 9 m s^{-1}). HiRes was a 14-day deployment on R/P *FLIP* moored approximately 25 km off the coast of Northern California in generally strong northwesterly winds (up to 17 m s^{-1}). They estimated the TKE dissipation rate through the entire wave-affected surface layer using a new infrared imaging technique for measuring TKE dissipation at the sea surface combined with traditional acoustic subsurface measurements. Furthermore, the infrared imagery allowed for resolving microbreakers and estimating their contribution to the breaking TKE dissipation rate. They concluded that total integrated TKE dissipation rates in the water column agreed well with TKE dissipation rates from breaking for developing to mature wind seas, $20 < c_m/u_* < 50$ (where c_m is the spectral mean wave phase speed and u_* is the atmospheric friction velocity and c_p/c_m is ~1.4), and that breaking was the dominant source of turbulence in those conditions. Using their measured results for the integrated water column dissipation [ordinate axis in Fig. 16 of Sutherland and Melville (2015)] and the fifth moment of the measured $\Lambda(c_b)$ [Fig. 6a in Sutherland and Melville (2015)], we calculated the corresponding

b_{eff} values for the RaDyO Hawaii, HiRes 2010, and SoCal 2010 sea state conditions up to $c_p/u_* = 51$. We note that $c_p/u_* > 35$ is beyond the nominal Pierson–Moskowitz transition from wind seas to swell.

c. *Spectral models*

Carefully validated spectral models allow merging results from an ensemble of wind speed and wave age case studies to predict global ensemble behavior. This can provide useful insights for unifying the trends of the various individual datasets with their often limited range of environmental conditions and different methodologies and uncertainties. Recent spectral wave models forecast spectral breaking wave properties in addition to the usual wave height spectra (Banner and Morison 2010; Morison and Banner 2016, manuscript submitted to *Ocean Modell.*; Romero et al. 2012).

Banner and Morison (2010) describe a threshold-based formulation for the breaking component of the dissipation rate source term S_{ds} within a broad bandwidth spectral wind wave model that significantly refined the formulation of Alves and Banner (2003). For computing the spectral evolution, an "exact" form of the nonlinear source function S_{nl} was used with a spectral wind input S_{in} term based on Janssen (1991). After a critical reassessment of the strengths of the S_{in} and S_{ds} source terms relative to S_{nl}, this model was able to reproduce measured dimensionless energy evolution, mean squared slope, directional spreading, wind stress, total water-side dissipation rates, and modeled with observed breaking properties in a field experiment (Jessup et al. 2002) where all of these variables were measured. The breaking wave forecast products comprised the breaker crest length distribution, $\Lambda(c)$, and spectral peak breaking strength, $b(c_p)$.

Romero et al. (2012) proposed a semiempirical determination of S_{ds} due to surface-wave breaking and a spectral model for the breaking strength parameter, $b(k)$. Their S_{ds} was based on closing the radiative transport equation for fetch-limited waves measured in the Gulf Of Tehuantepec Experiment (GOTEX) using the measured fetch evolution of the directional spectra, computations of S_{nl} and three models of the wind input source function. The form of $b(k)$ was inferred from Kleiss and Melville's (2010) kinematic breaking measurements and their inferred S_{ds} term, resulting in $b = b(k; c_p/u_*)$, where c_p/u_* is the wave age. A model for $b(k; c_p/u_*)$ is proposed that extrapolates an inertial wave dissipation scaling based on laboratory measurements to the field, using spectral saturation to quantify spectral steepness. This model forecasts $\Lambda(c)$ and the corresponding spectral breaking strength $b(c)$ for different values (0.8, 0.9, and 1.0) of the breaker speed slowdown parameter, α (Banner et al. 2014a). We determined the modeled b_{eff} for Romero et al. (2012) using the results in their Figs. 14g–i for α equal to 1.0 above k/k_{bp} equals 1, where k_{bp} is the peak in $b(k)$.

Sutherland and Melville (2015) applied the Romero et al. (2012) model for the wind sea conditions appropriate to their observations. Note that the modeled $\Lambda(c)$ values were not available for this estimation of modeled b_{eff}. We used their computed results of the energy dissipation by wave breaking [abscissa axis in Fig. 16 in Sutherland and Melville (2015)] and the fifth moment of the measured $\Lambda(c_b)$ [Fig. 6a in Sutherland and Melville (2015)] to estimate the corresponding modeled b_{eff} values for the RaDyO Hawaii, HiRes 2010, and SoCal 2010 sea state conditions up to c_p/u_* of 51.

Morison and Banner (2016, manuscript submitted to *Ocean Modell.*) further refine the source terms and extends the Banner and Morison (2010) results to a very broad range of wind speeds and wave ages. The spectral breaking properties are derived from S_{ds} using a model formulation for $b(k)$ that follows in the spirit of Romero et al. (2012) but uses a different functional form based on measured saturation thresholds determined from field data alone. Validation is achieved by comparing forecast and observed Λ distributions. The model also computes b_{eff} from Eq. (4). For consistency with Romero et al. (2012), Morison and Banner (2016, manuscript submitted to *Ocean Modell.*) used a slowdown parameter $\alpha = 1.0$. Of particular relevance to the present study is their resulting compilation of modeled b_{eff} against wave age c_p/u_* for a wide range of sea state conditions.

3. Results

In this section, we compile the limited available datasets for measured b_{eff} in the field. Additionally, we supplement these with an ensemble of modeled b_{eff} values computed for a broad range of wind speeds and wave ages. This synergy of results aims to demonstrate the behavior of b_{eff} with wave age that allows for a compact quasi-universal parameterization of b_{eff}.

a. *Dependence of b_{eff} on wave age during field experiments*

Figure 1 shows the effective breaking strength, b_{eff}, versus wave age (c_p/u_*) measured for the eight field experiments described in section 2b. The RaDyO experiment in the Pacific Ocean near Hawaii included two specific datasets (Gemmrich et al. 2013; Sutherland and Melville 2015). We collated these nine datasets spanning a wind speed ranging from 2 to 18 m s^{-1} and a wave age ranging from approximately 10 to 80. We note

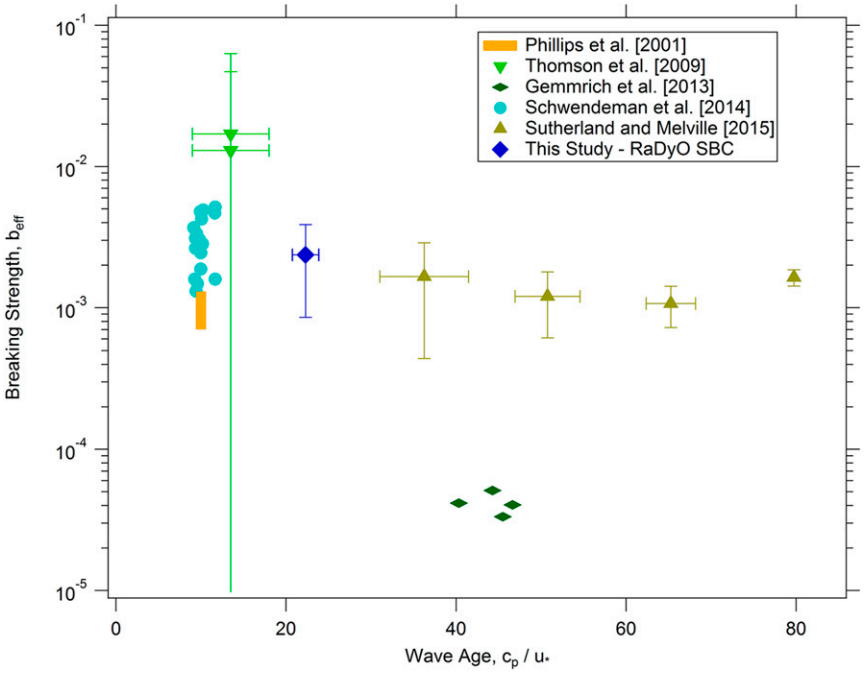

FIG. 1. Effective breaking strength parameter b_{eff} plotted against wave age c_p/u_* for each of the experiments in the datasets detailed in the legend. Where available, the error bounds are indicated.

that some of these experiments included data for older seas that are not shown. The error bars plotted for Sutherland and Melville (2015) and for RaDyO SBC (this study) reflect the standard deviation arising solely from variability in the estimates of the TKE dissipation rate. The key result highlighted in this figure is the modest decrease in b_{eff} with wave age for the field measurements.

Another feature of the field measurements highlighted in Fig. 1 is the order of magnitude smaller b_{eff} levels reported by Gemmrich et al. (2013) compared to Sutherland and Melville (2015) for the same experiment (RaDyO Pacific Ocean near Hawaii). We have confirmed that the integrated fifth moments of $\Lambda(c_b)$ determined by (Sutherland and Melville 2013, 2015) and Banner et al. (2014b) are within a factor of 2. Hence the order of magnitude difference in b_{eff} between Sutherland and Melville (2015) and Gemmrich et al. (2013) is related primarily to the difference in their measured ε levels.

The turbulence measurements used in Gemmrich et al. (2013) were published and analyzed in Vagle et al. (2012). The integrated values of TKE dissipation rate for the specific times during breaking measurements shown in Fig. 11 of Gemmrich et al. (2013) ranged from 1.5 to $5.5 \times 10^{-5}\,\text{m}^3\,\text{s}^{-3}$ within the top 1.5 m of the water column. These data from Vagle et al. (2012) show average dissipation rate values during the whole experiment were 6×10^{-5} to $6 \times 10^{-6}\,\text{m}^2\,\text{s}^{-3}$ between 0.14- to 0.75-m depths and were 6×10^{-4} to $6 \times 10^{-5}\,\text{m}^2\,\text{s}^{-3}$ between 1.04- to 1.76-m depths. Specifically, lower TKE dissipation rates were observed closer to the surface than immediately below. However, Fig. 10 in Sutherland and Melville (2015) shows their RaDyO TKE dissipation rate measurements in the top meter to be on average $\sim 5 \times 10^{-4}\,\text{m}^2\,\text{s}^{-3}$ during the same time period, decreasing from 8×10^{-4} to $8 \times 10^{-5}\,\text{m}^2\,\text{s}^{-3}$ over the depth range from 0.13 to 0.87 m. It is important to note here that the TKE dissipation rate measurements of Vagle et al. (2012) and Gemmrich et al. (2013) were in a wave-following reference frame as were the measurements of Sutherland and Melville (2015). Remarkably, Vagle et al. (2012) report TKE dissipation rates in the same depth range (0.14 to 0.75 m) on the same days to be $\sim 5 \times 10^{-5}\,\text{m}^2\,\text{s}^{-3}$, about an order of magnitude lower than observed by Sutherland and Melville (2015). Vagle et al. (2012) highlight their finding that the dissipation at greater depths (1.04 to 1.76 m) was greater than near the surface, but this level of variability was not reported by Sutherland and Melville (2015). Overall, the dissipation estimates in the wave boundary layer given by Sutherland and Melville (2015) are a factor of 10 greater than for Vagle et al. (2012), which is the major reason for the difference in the b_{eff} levels of Gemmrich et al. (2013) and Sutherland and Melville (2015). The source of this discrepancy needs to

be better understood through future measurements including more diverse instrument arrays that investigate different turbulence sensors and sampling techniques.

In the context of the other datasets, Gemmrich et al.'s (2013) data appear to be systematically low and until the source of the discrepancy is resolved, we have tentatively chosen to parameterize the data excluding this dataset. Furthermore, Schwendeman et al. (2014) point out that the Thomson et al. (2009) values for b_{eff} are not valid due to the video missing some of the short whitecaps causing a reduction of $\Lambda(c_b)$ and an overestimate of b_{eff}. Data from Phillips et al. (2001) and Gemmrich et al. (2008) are not included subsequently since the TKE dissipation rate in their studies was indirectly estimated from scaling arguments rather than direct measurements. Finally, the Schwendeman et al. (2014) data have been consolidated to a single point since no intrinsic trend in the wave age data is observed and the error bars reflect the standard deviation arising solely from variability in the estimates of b_{eff} and wave age.

b. Parameterization of b_{eff} with wave age

On the basis of the results shown in Fig. 1 (with the exclusions noted above), we propose the following linear relationship for b_{eff} in Fig. 2a for use in applications:

$$b_{\text{eff}} = A + B\frac{c_p}{u_*}, \tag{6}$$

based on the apparent primary dependence on wave age (c_p/u_*), where $A = 3.482 \times 10^{-3}$ ($\pm 6.481 \times 10^{-4}$) and $B = -4.691 \times 10^{-5}$ ($\pm 1.935 \times 10^{-5}$). The error bounds correspond to the 95% confidence intervals. The R^2 value is 0.98 and the root-mean-squared error (RMSE) is 1.37×10^{-4}. The t statistic for the slope B was found to be -10.43, which confirms that B is significantly different from zero at the 99.5% confidence level. The F statistic for a linear model versus a constant was found to be 108.79 with a p value of 0.009 07. This further confirms that the linear model in Eq. (6) provides an improved statistical fit compared with a constant at the 99% confidence level. Note that the parameterization in Eq. (6) is valid for wave ages 50 and below for reasons discussed in section 4a.

We used the wave model results to investigate whether a robust dependence could be obtained over a wide range of wind speeds. The model predictions described in section 2c from Romero et al. (2012), Sutherland and Melville (2015), and Morison and Banner (2016, manuscript submitted to *Ocean Modell.*) have been added to the field data (with the previous exclusions) in Fig. 2b. The Romero et al. (2012) and Sutherland and Melville (2015) model results provide a good fit to the field data, as do the model results of Morison and Banner (2016, manuscript submitted to *Ocean Modell.*). The latter additionally provide a robust prediction that the observed tight wave age dependence is maintained over a wide range of wind speeds. These results support the adoption of a single parameter relationship between b_{eff} and wave age for use in global predictive models, as discussed in detail below.

c. Dependence of b_{eff} on significant wave steepness

An allied result that arose from this study is the possibility of using a wave parameter alone to correlate b_{eff}. We found that the significant wave steepness $H_s k_p/2$ of the wind sea provided this possibility, where H_s is significant wave height and k_p is the wavenumber of the waves at the spectral peak. Figure 3 shows the (a) observed and (b) modeled variation of these parameters over a wide range of wind conditions. Note here that the Schwendeman et al. (2014) data have been consolidated to two representative points to reflect the apparent clustering in the significant wave steepness data. It is seen that a strong correlation exists, which could be used in applications where only wave conditions are available. On the basis of the results shown in Fig. 3 (with the previous exclusions), we propose the following linear relationship for b_{eff} for use in applications:

$$b_{\text{eff}} = C + D\frac{H_s k_p}{2}, \tag{7}$$

based on the apparent primary dependence on significant wave steepness ($H_s k_p/2$), where $C = 2.108 \times 10^{-5}$ ($\pm 2.538 \times 10^{-3}$) and $D = 1.534 \times 10^{-2}$ ($\pm 1.640 \times 10^{-2}$). The error bounds are the 95% confidence intervals. The R^2 value is 0.75 and the root-mean-squared error is 5.06×10^{-4}. The t statistic for the slope D was found to be 2.98, which confirms D is significantly different from zero at the 95% confidence level. The F statistic for linear model versus a constant was found to be 8.86 with a p value of 0.0588, which confirms that the linear model in Eq. (7) provides an improved statistical fit compared with a constant at the 90% confidence level.

4. Discussion

a. Recommendations

We have shown statistically that b_{eff} is linearly dependent on both wave age and significant wave steepness. A wave-age-based parameterization has been shown to be the more robust and should be used whenever wave statistics are available. If no wave statistics are available, a constant value for b_{eff} of 2.082×10^{-3} ($\pm 8.321 \times 10^{-4}$) is recommended.

To be clear, this parameterization for b_{eff} is only valid when wave breaking is the dominant process contributing to the ε. In Fig. 2b, the impact of breaking on b_{eff} is

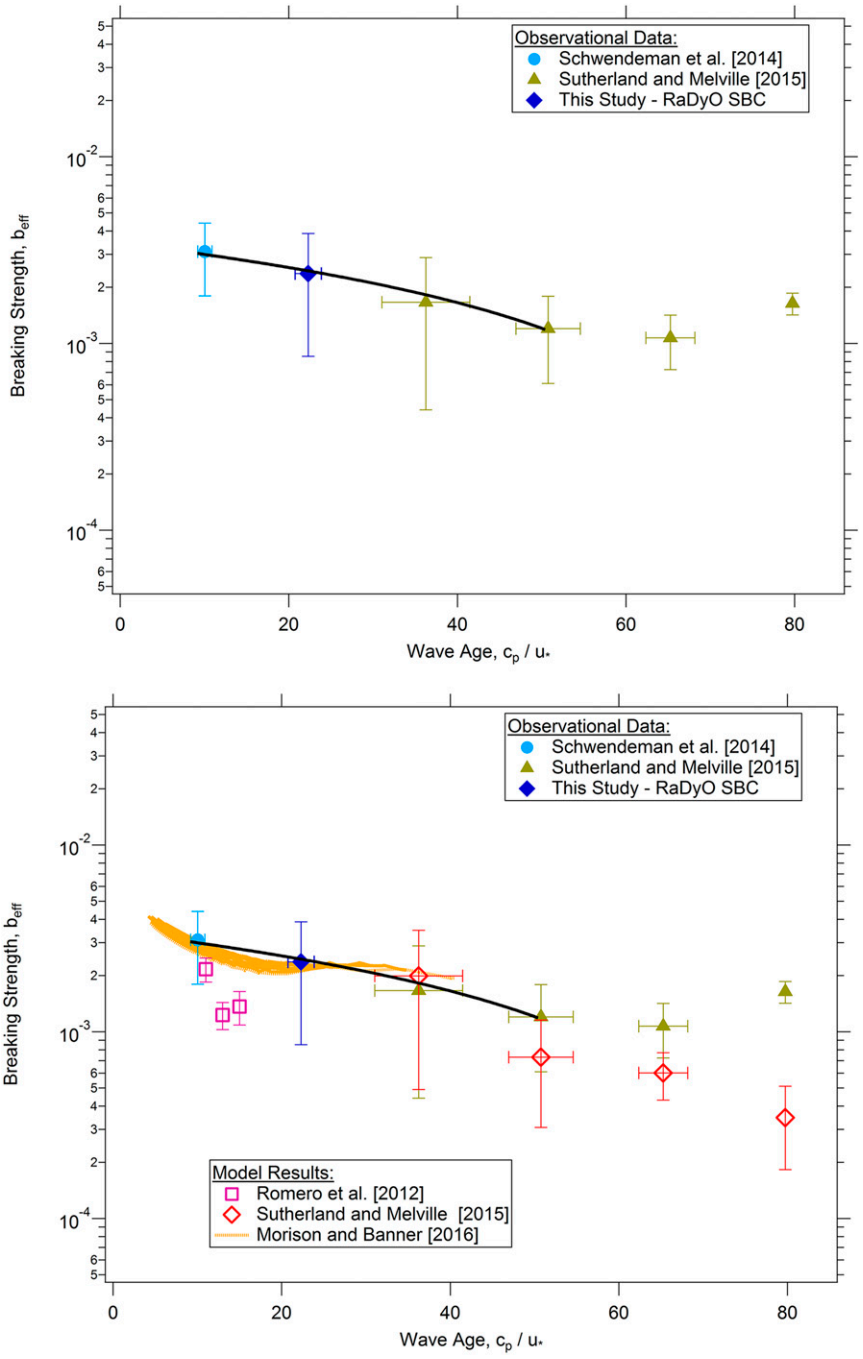

FIG. 2. (top) Effective breaking strength parameter b_{eff} plotted against wave age c_p/u_* for the selected subset of field experiments shown in the upper legend, chosen using the rationale in section 3a of the text. The error bounds are indicated. (bottom) As in (top), but showing modeled results. Morison and Banner's (2016, manuscript submitted to *Ocean Modell.*) model results correspond to wind speeds ranging from 6 to 24 m s^{-1}. Romero et al. (2012) show mean and standard deviation for the reported wind input functions. The solid black line shows the least squares best-fit linear correlation [Eq. (6)] to the shown measured b_{eff} field data points.

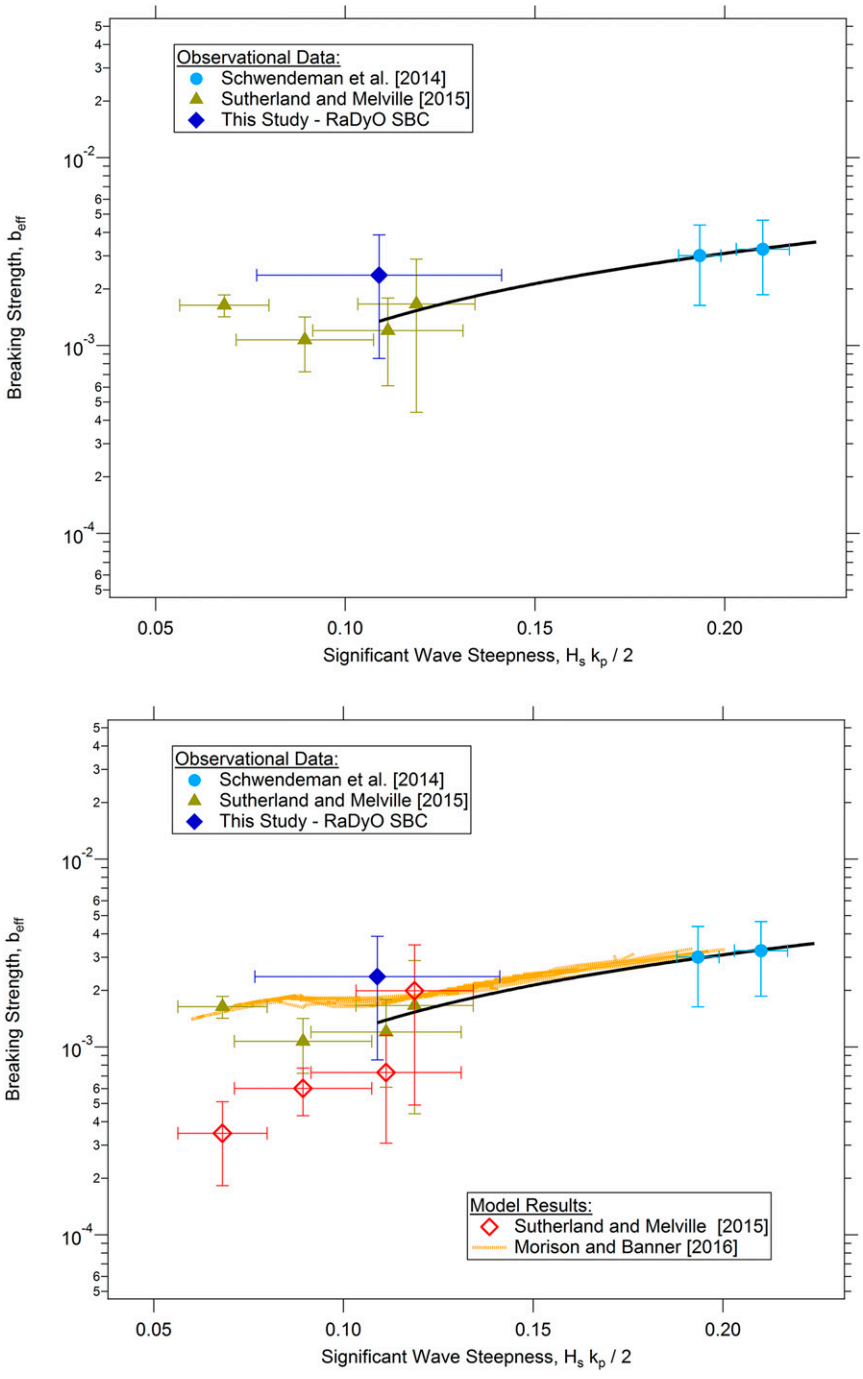

FIG. 3. As in Fig. 2, but plotted against significant wave steepness $H_s k_p/2$. The solid black line shows the least squares best-fit linear correlation [Eq. (7)] to the shown measured b_{eff} field data points.

strongly reduced for wave age greater than 50 and is more heavily controlled by background processes according to Fig. 16 in Sutherland and Melville (2015). Simultaneously, the dissipation rate in Fig. 13 in Sutherland and Melville (2015) is shown to increase with wave age. These coupled observations are highlighted in Fig. 2b, which shows that the measured b_{eff} is significantly greater than the modeled value for wave age greater than 50. Note that the modeled value only includes effects from breaking whereas the measured value includes all processes. The combined results of Sutherland and Melville (2013) and Sutherland and

Melville (2015) show that the measured integrated water column dissipation in the wave boundary layer is greater than the directly modeled integrated S_{ds}, which is greater than the dissipation by breaking according to the Phillips framework $[b_{\text{eff}}\rho g^{-1}\int_c c_b^5\Lambda(c_b)\,dc_b]$ at high wave age. Therefore, the Phillips framework for b_{eff} in Eq. (5) and parameterized in Eq. (6) breaks down above wave age 50. Use of b_{eff} should be restricted to wave ages $c_p/u_* \sim 50$ and below. At larger wave age, the breaking contribution becomes a decreasing fraction of the total dissipation and the use of b_{eff} and Eq. (5) will overestimate the breaking contribution. The b_{eff} modeling is consistent with this observation.

The breaking strength parameter has been observed in laboratory wave tank studies of breaking waves to depend on a predicted linear maximum slope of the focused 2D wave packets. For broad-banded ocean wave spectra, the spectral breaking strength, $b(k)$, can then be formulated in terms of spectral saturation of the wave field [as in Romero et al. (2012)]. In fetch-limited cases, the entire form of the spectra can then be related to wave age and peak wave steepness. In those cases, it is reasonable to expect that b_{eff} [which corresponds to an average of $b(k)$] could also be related to wave age. In more complicated sea states, the relationship between wave age and the spectral form is less clear. In such cases, the spectral saturation has been proposed as a plausible alternative and is independent of the spectral peak.

It is important to use wind-wave or equilibrium-range statistics wherever possible, especially in complicated sea states. Wind-wave statistics may be obtained by carefully separating the wind-wave signature from 2D spectra (Hanson and Phillips 2001; Portilla et al. 2009). Results presented here are limited by the published datasets and are not exclusively based on pure wind sea statistics. Indeed, the data from Sutherland and Melville (2015) are for more complicated sea states. They used a mean phase speed, c_m, rather than the peak, c_p, and found a relationship between c_m and c_p that we implemented here.

Schwendeman et al. (2014) and Schwendeman and Thomson (2015) suggest that the mean-squared slope (mss) in the equilibrium range is another appropriate wave statistic. However, Schwendeman et al. (2014) fetch-limited data for b_{eff} show no correlation with significant wave steepness or mss. The more recent work by Schwendeman and Thomson (2015) investigating whitecap fraction shows a very slight improvement in correlation and RMSE with mss over significant wave steepness and the same correlation and RMSE with wave age in order to explain the residual variability from a wind speed parameterization of whitecap fraction. At present it is difficult to gauge the usefulness of mss for predicting b_{eff} since Schwendeman and Thomson (2015) do not show the relationship between TKE dissipation rate and mss, but only the fact that the TKE dissipation rate is highly correlated with wave age. Nevertheless, the fact that both whitecapping and TKE dissipation rate are predicted by wave age provides confidence in the validity of Eq. (6).

Future studies could include further investigation of the wind-sea only dependent mss (Schwendeman and Thomson 2015; Schwendeman et al. 2014), c_m (Sutherland and Melville 2015), or other appropriate wave statistics. Additionally, Sutherland and Melville (2013) propose scaling relationships for $\Lambda(c)$ based on dimensional analysis that include combined power laws for wave age, significant wave steepness, and Froude number based on ballistic velocity. Nondimensional fetch may also be important for fetch-limited cases as in Kleiss and Melville (2010). An extension of the work presented here should examine and target these various 2D wave spectral statistics and nondimensional scalings in future validations of b_{eff}.

b. *Factors influencing b_{eff} determinations*

A consensus in the structure of $\Lambda(c)$ and a reduction in the uncertainty in the measurements appear to be emerging. These have been achieved using high-resolution visible and infrared imaging, more stable and diverse platforms, and more comprehensive fields of view. Substantial progress has been made in quantifying breaking with respect to scale for the kinematics from geometric considerations (Sutherland and Melville 2015). Inferring the turbulent energy dissipation rate from these kinematic estimates of breaking is important for air–sea interaction and still requires further refinement and validation.

The accuracy of b_{eff} is dependent on the measurement bandwidth, the processing bandwidth [i.e., discrete wave (Gemmrich et al. 2013; Kleiss and Melville 2010, 2011) vs Fourier (Thomson and Jessup 2009) processing] and computational methodology (Banner et al. 2014b). Earlier efforts to capture whitecapping on all scales were compromised due to the lack of image resolution, suggesting that the smallest whitecaps may have been underestimated (Schwendeman et al. 2014). Furthermore, Sutherland and Melville (2015) assert that microbreaking can make important contributions to $\mathbf{\Lambda}(c)$. Not accounting for the smallest whitecaps or microbreaking may cause an underestimate of the fifth moment of $\Lambda(c)$ and therefore overestimate b_{eff}.

As noted above, b_{eff} is applicable to wind-driven seas with active breaking within the spectrum, for which the TKE dissipation rate due to breaking is assumed to

dominate over the background. Sutherland and Melville (2015) suggest their measurements indicate that breaking is the main mechanism for the excess of TKE dissipation rate above the wall layer. From our modeling for young wind seas (Morison and Banner 2016, manuscript submitted to *Ocean Modell.*), the TKE dissipation rate due to breaking is approximately 90% of the total, but this reduces to 50%–60% approaching the swell transition limit ($U_{10}/c_p \sim 0.83$; Komen et al. 1984). Beyond this limit, nonlinear hydrodynamic spectral transfer becomes the primary driver for spectral peak evolution rather than wind forcing. On this basis, we suggest that b_{eff} may have an additional uncertainty of a factor of 2 for older wind seas.

c. *Applications for b_{eff}*

The availability of a robust parameterization for b_{eff} enables a range of geophysical products useful for various air–sea interaction applications. These geophysical products include the total whitecap fraction, W, comprised of bubbles generated during active "stage A" wave breaking as well as postbreaking "stage B" whitecap fraction. The latter includes both residual surface foam and rising bubbles that have surfaced due to buoyancy. Primarily, it is the active portion of the whitecap fraction (W_A) that needs to be considered to deduce dynamical processes such as momentum flux and turbulent mixing associated with breaking waves. The time scale T for stage A whitecapping is on the order of half a wave period (Kleiss and Melville 2011) whereas the time scale for stage B depends on bubble-size distribution, water temperature, ocean stratification, surfactants, and atmospheric stability. The momentum flux and TKE dissipation rate from the waves to the upper ocean are additional geophysical products that are determined from the fourth and fifth moments of $\Lambda(\mathbf{c})$ weighted by b_{eff}.

Using the proposed framework, these geophysical products can be determined operationally or for research purposes from remote sensing instruments deployed from satellites, aircraft, or ocean-going/fixed platforms. A possible method to generate global maps of W_A from satellite data has been proposed recently by Anguelova and Hwang (2016). P85 pointed out that combining the first moment of $\Lambda(c)$ with the duration of the active breaking $T(c)$ at scale c provides the active whitecap cover:

$$W_A = \int_c T(c) c \Lambda(c)\, dc. \tag{8}$$

Anguelova and Hwang (2016) derive an approximation to the whitecap cover in Eq. (8) to obtain W_A based on $S_{\text{ds}}(c)$ instead of $\Lambda(c)$, which intrinsically involves b_{eff}. This seeks to bypass the need for breaking wave measurements and only requires buoy measurements and a parametric model for the energy dissipation (e.g., Hanson and Phillips 1999; Hwang and Sletten 2008) to determine $W_A(\varepsilon)$. Their sensitivity analysis demonstrates that b_{eff} has the largest impact on the $W_A(\varepsilon)$ estimates compared to bubble persistence and threshold breaker speed.

Potential applications include, but are not limited to, the following:

(a) In coupled atmosphere–wave–circulation forecast models, remote measurements using the [b_{eff}, $\Lambda(c)$] framework are potentially very valuable for validating ε, especially in the context of coupled wave–circulation modeling, where wave field inputs play a strong role in the upper ocean circulation. Key inputs are the dissipation rate and momentum flux from the breaking waves [respectively, the b_{eff} -weighted fifth and fourth moments of $\Lambda(c)$]. The momentum flux from the breaking waves to the circulation also provides a useful indicator for the atmospheric wind stress level.

(b) In studies of air–sea gas exchange, actively breaking crests form the stage A whitecap fraction that is critical for determining the bubble-mediated effects of gas transfer, especially for the gases of varying sparingly solubility. Furthermore, the TKE dissipation rate governs the gas transfer velocity for gases of high solubility and moderately forced wind waves without whitecapping for gases of sparing solubility. Evidence from the Southern Ocean Gas Exchange Experiment (SOGasEx) (Zappa et al. 2016, manuscript submitted to *J. Geophys. Res.*) suggests strongly that the actively breaking crest region whitecap cover (W_A) of breaking waves is important to air–sea gas fluxes.

(c) Total whitecap fraction (W) may be used to determine bubble-mediated sea spray aerosol production and heat exchange (Andreas 1998; de Leeuw et al. 2011).

5. Conclusions

In the Phillips (1985) spectral framework, the geometric/kinematic properties of breaking ocean waves require a scale-dependent (spectral) breaking strength coefficient to provide the associated excess energy and momentum fluxes from the waves to the upper ocean. In this context, we investigated the feasibility of a parametric mean effective breaking strength coefficient b_{eff} valid for a wide range of sea states. Our analysis of available ocean

breaking wave datasets, complemented with wave model behavior, provides strong support for a robust single parameter relationship between b_{eff} and wave age or significant wave steepness over a wide range of wind speeds. Illustrative air–sea interaction forecast/hindcast applications are described that should benefit from the availability of such relationships.

Acknowledgments. This work was funded by the Office of Naval Research under the Radiance in a Dynamic Ocean (RaDyO) DRI, with Grants N00014-06-1-0372 and N00014-11-1-0168 (C. Zappa) and N00014-06-1-0047 and N00014-11-1-0054 (M. Banner and R. Morison), as well as Grant N00014-10-1-0390 for M. Banner and R. Morison under the NOPP DRI ''Improving Wind Wave Predictions: Global to Regional Scales.'' S. Brumer was funded by the National Science Foundation Grant OCE-1537890.

REFERENCES

Agrawal, Y. C., E. A. Terray, M. A. Donelan, P. A. Hwang, A. J. Williams III, W. M. Drennan, K. K. Kahma, and S. A. Krtaigorodskii, 1992: Enhanced dissipation of kinetic energy beneath surface waves. *Nature*, **359**, 219–220, doi:10.1038/359219a0.

Alves, J. H., and M. L. Banner, 2003: Performance of a saturation-based dissipation source term for wind wave spectral modelling. *J. Phys. Oceanogr.*, **33**, 1274–1298, doi:10.1175/1520-0485(2003)033<1274:POASDS>2.0.CO;2.

Andreas, E. L, 1998: A new sea spray generation function for wind speeds up to 32 m s^{-1}. *J. Phys. Oceanogr.*, **28**, 2175–2184, doi:10.1175/1520-0485(1998)028<2175:ANSSGF>2.0.CO;2.

Anguelova, M. D., and F. Webster, 2006: Whitecap coverage from satellite measurements: A first step toward modeling the variability of oceanic whitecaps. *J. Geophys. Res.*, **111**, C03017, doi:10.1029/2005JC003158.

——, and P. A. Hwang, 2016: Using energy dissipation rate to obtain active whitecap fraction. *J. Phys. Oceanogr.*, **46**, 461–481, doi:10.1175/JPO-D-15-0069.1.

Ardhuin, F., B. Chapron, and F. Collard, 2009: Observation of swell dissipation across oceans. *Geophys. Res. Lett.*, **36**, L06607, doi:10.1029/2008GL037030.

Asher, W. E., and R. Wanninkhof, 1998a: Transient tracers and air–sea gas transfer. *J. Geophys. Res.*, **103**, 15 939–15 958, doi:10.1029/98JC00379.

——, and ——, 1998b: The effect of bubble-mediated gas transfer on purposeful dual-gaseous tracer experiments. *J. Geophys. Res.*, **103**, 10 555–10 560, doi:10.1029/98JC00245.

Banner, M. L., and W. L. Peirson, 2007: Wave breaking onset and strength for two-dimensional deep water wave groups. *J. Fluid Mech.*, **585**, 93–115, doi:10.1017/S0022112007006568.

——, and R. P. Morison, 2010: Refined source terms in wind wave models with explicit wave breaking forecasts. Part I. Model framework and validation against field data. *Ocean Modell.*, **33**, 177–189, doi:10.1016/j.ocemod.2010.01.002.

——, X. Barthelemy, F. Fedele, M. Allis, A. Benetazzo, F. Dias, and W. L. Peirson, 2014a: Linking reduced breaking crest speeds to unsteady nonlinear water wave group behavior. *Phys. Rev. Lett.*, **112**, 114502, doi:10.1103/PhysRevLett.112.114502.

——, C. J. Zappa, and J. Gemmrich, 2014b: A note on Phillips' spectral framework for ocean whitecaps. *J. Phys. Oceanogr.*, **44**, 1727–1734, doi:10.1175/JPO-D-13-0126.1.

de Leeuw, G., E. L Andreas, M. D. Anguelova, C. W. Fairall, E. R. Lewis, C. O'Dowd, M. Schulz, and S. E. Schwartz, 2011: Production flux of sea spray aerosol. *Rev. Geophys.*, **49**, RG2001, doi:10.1029/2010RG000349.

Dickey, T., G. Kattawar, and K. Voss, 2011: Shedding new light on light in the ocean. *Phys. Today*, **64**, 44–50, doi:10.1063/1.3580492.

——, and Coauthors, 2012: Introduction to special section on recent advances in the study of optical variability in the near-surface and upper ocean. *J. Geophys. Res.*, **117**, C00H20, doi:10.1029/2012JC007964.

Drazen, D. A., W. K. Melville, and L. Lenain, 2008: Inertial scaling of dissipation in unsteady breaking waves. *J. Fluid Mech.*, **611**, 307–332, doi:10.1017/S0022112008002826.

Gemmrich, J. R., 2010: Strong turbulence in the wave crest region. *J. Phys. Oceanogr.*, **40**, 583–595, doi:10.1175/2009JPO4179.1.

——, M. L. Banner, and C. Garrett, 2008: Spectrally resolved energy dissipation and momentum flux of breaking waves. *J. Phys. Oceanogr.*, **38**, 1296–1312, doi:10.1175/2007JPO3762.1.

——, C. J. Zappa, M. L. Banner, and R. P. Morison, 2013: Wave breaking in developing and mature seas. *J. Geophys. Res. Oceans.*, **118**, 4542–4552, doi:10.1002/jgrc.20334.

Hanson, J. L., and O. M. Phillips, 1999: Wind sea growth and dissipation in the open ocean. *J. Phys. Oceanogr.*, **29**, 1633–1648, doi:10.1175/1520-0485(1999)029<1633:WSGADI>2.0.CO;2.

——, and ——, 2001: Automated analysis of ocean surface directional wave spectra. *J. Atmos. Oceanic Technol.*, **18**, 277–293, doi:10.1175/1520-0426(2001)018<0277:AAOOSD>2.0.CO;2.

Hwang, P. A., 2012: Foam and roughness effects on passive microwave remote sensing of the ocean. *IEEE Trans. Geosci. Remote Sens.*, **50**, 2978–2985, doi:10.1109/TGRS.2011.2177666.

——, and M. A. Sletten, 2008: Energy dissipation of wind-generated waves and whitecap coverages. *J. Geophys. Res.*, **113**, C02012, doi:10.1029/2007JC004277.

——, ——, and J. V. Toporkov, 2008: Analysis of radar sea return for breaking wave investigation. *J. Geophys. Res.*, **113**, C02003, doi:10.1029/2007JC004319.

Janssen, P. A. E. M., 1991: Quasi-linear theory of wind-wave generation applied to wave forecasting. *J. Phys. Oceanogr.*, **21**, 1631–1642, doi:10.1175/1520-0485(1991)021<1631:QLTOWW>2.0.CO;2.

Jessup, A. T., and Coauthors, 2002: The FAIRS experiment. IEEE Geoscience and Remote Sensing Society Newsletter, Vol. 123, IEEE, New York, NY, 12–17.

Keeling, R. F., 1993: On the role of large bubbles in air–sea gas exchange and supersaturation in the ocean. *J. Mar. Res.*, **51**, 237–271, doi:10.1357/0022240933223800.

Kleiss, J. M., and W. K. Melville, 2010: Observations of wave breaking kinematics in fetch-limited seas. *J. Phys. Oceanogr.*, **40**, 2575–2604, doi:10.1175/2010JPO4383.1.

——, and ——, 2011: The analysis of sea surface imagery for whitecap kinematics. *J. Atmos. Oceanic Technol.*, **28**, 219–243, doi:10.1175/2010JTECHO744.1.

Komen, G. J., S. Hasselmann, and K. Hasselmann, 1984: On the existence of a fully developed wind-sea spectrum. *J. Phys. Oceanogr.*, **14**, 1271–1285, doi:10.1175/1520-0485(1984)014<1271:OTEOAF>2.0.CO;2.

——, L. Cavaleri, M. A. Donelan, K. Hasselmann, S. Hasselmann, and P. A. E. M. Janssen, 1994: *Dynamics and Modelling of Ocean Waves*. Cambridge University Press, 532 pp.

Kukulka, T., and T. Hara, 2008a: The effect of breaking waves on a coupled model of wind and ocean surface waves. Part I: Mature seas. *J. Phys. Oceanogr.*, **38**, 2145–2163, doi:10.1175/2008JPO3961.1.

——, and ——, 2008b: The effect of breaking waves on a coupled model of wind and ocean surface waves. Part II: Growing seas. *J. Phys. Oceanogr.*, **38**, 2164–2184, doi:10.1175/2008JPO3962.1.

Melville, W. K., 1994: Energy dissipation by breaking waves. *J. Phys. Oceanogr.*, **24**, 2041–2049, doi:10.1175/1520-0485(1994)024<2041:EDBBW>2.0.CO;2.

Merlivat, L., and L. Mémery, 1983: Gas exchange across an air–water interface: Experimental results and modeling of bubble contribution to transfer. *J. Geophys. Res.*, **88**, 707–724, doi:10.1029/JC088iC01p00707.

Mueller, J., and F. Veron, 2009a: Nonlinear formulation of the bulk surface stress over breaking waves: Feedback mechanisms from air-flow separation. *Bound.-Layer Meteor.*, **130**, 117–134, doi:10.1007/s10546-008-9334-6.

——, and ——, 2009b: A sea state–dependent spume generation function. *J. Phys. Oceanogr.*, **39**, 2363–2372, doi:10.1175/2009JPO4113.1.

Perlin, M., W. Choi, and Z. Tian, 2013: Breaking waves in deep and intermediate waters. *Annu. Rev. Fluid Mech.*, **45**, 115–145, doi:10.1146/annurev-fluid-011212-140721.

Phillips, O. M., 1985: Spectral and statistical properties of the equilibrium range in wind-generated gravity waves. *J. Fluid Mech.*, **156**, 505–531, doi:10.1017/S0022112085002221.

——, F. L. Posner, and J. P. Hansen, 2001: High range resolution radar measurements of the speed distribution of breaking events in wind-generated ocean waves: Surface impulse and wave energy dissipation rates. *J. Phys. Oceanogr.*, **31**, 450–460, doi:10.1175/1520-0485(2001)031<0450:HRRRMO>2.0.CO;2.

Portilla, J., F. J. Ocampo-Torres, and J. Monbaliu, 2009: Spectral partitioning and identification of wind sea and swell. *J. Atmos. Oceanic Technol.*, **26**, 107–122, doi:10.1175/2008JTECHO609.1.

Reul, N., and B. Chapron, 2003: A model of sea-foam thickness distribution for passive microwave remote sensing applications. *J. Geophys. Res.*, **108**, 3321, doi:10.1029/2003JC001887.

——, H. Branger, and J.-P. Giovanangeli, 2008: Air flow structure over short-gravity breaking water waves. *Bound.-Layer Meteor.*, **126**, 477–505, doi:10.1007/s10546-007-9240-3.

Romero, L., W. K. Melville, and J. Kleiss, 2012: Spectral energy dissipation due to surface-wave breaking. *J. Phys. Oceanogr.*, **42**, 1421–1444, doi:10.1175/JPO-D-11-072.1.

Schwendeman, M., and J. Thomson, 2015: Observations of whitecap coverage and the relation to wind stress, wave slope, and turbulent dissipation. *J. Geophys. Res. Oceans.*, **120**, 8346–8363, doi:10.1002/2015JC011196.

——, ——, and J. R. Gemmrich, 2014: Wave breaking dissipation in a young wind sea. *J. Phys. Oceanogr.*, **44**, 104–127, doi:10.1175/JPO-D-12-0237.1.

Sullivan, P. P., and J. C. McWilliams, 2010: Dynamics of winds and currents coupled to surface waves. *Annu. Rev. Fluid Mech.*, **42**, 19–42, doi:10.1146/annurev-fluid-121108-145541.

Sutherland, P., and W. K. Melville, 2013: Field measurements and scaling of ocean surface wave-breaking statistics. *Geophys. Res. Lett.*, **40**, 3074–3079, doi:10.1002/grl.50584.

——, and ——, 2015: Field measurements of surface and near-surface turbulence in the presence of breaking waves. *J. Phys. Oceanogr.*, **45**, 943–965, doi:10.1175/JPO-D-14-0133.1.

Terray, E. A., and Coauthors, 1996: Estimates of kinetic energy dissipation under surface waves. *J. Phys. Oceanogr.*, **26**, 792–807, doi:10.1175/1520-0485(1996)026<0792:EOKEDU>2.0.CO;2.

Thais, L., and J. Magnaudet, 1996: Turbulent structure beneath surface gravity waves sheared by the wind. *J. Fluid Mech.*, **328**, 313–344, doi:10.1017/S0022112096008749.

Thomson, J., and A. Jessup, 2009: A Fourier-based method for the distribution of breaking crests from video observations. *J. Atmos. Oceanic Technol.*, **26**, 1663–1671, doi:10.1175/2009JTECHO622.1.

——, J. R. Gemmrich, and A. T. Jessup, 2009: Energy dissipation and the spectral distribution of whitecaps. *Geophys. Res. Lett.*, **36**, L11601, doi:10.1029/2009GL038201.

Tian, Z., M. Perlin, and W. Choi, 2010: Energy dissipation in two-dimensional unsteady plunging breakers and an eddy viscosity model. *J. Fluid Mech.*, **655**, 217–257, doi:10.1017/S0022112010000832.

Vagle, S., J. Gemmrich, and H. Czerski, 2012: Reduced upper ocean turbulence and changes to bubble size distributions during large downward heat flux events. *J. Geophys. Res.*, **117**, C00H16, doi:10.1029/2011JC007308.

Veron, F., and W. K. Melville, 2001: Experiments on the stability and transition of wind-driven water surfaces. *J. Fluid Mech.*, **446**, 25–65.

——, G. Saxena, and S. Misra, 2007: Measurements of viscous tangential stresses in the separated airflow above wind waves. *Geophys. Res. Lett.*, **34**, L19603, doi:10.1029/2007GL031242.

Woolf, D. K., 1993: Bubbles and the air–sea transfer velocity of gases. *Atmos.–Ocean*, **31**, 517–540, doi:10.1080/07055900.1993.9649484.

——, 2005: Parameterization of gas transfer velocities and sea-state-dependent wave breaking. *Tellus*, **57B**, 87–94, doi:10.1111/j.1600-0889.2005.00139.x.

Zappa, C. J., M. L. Banner, H. Schultz, J. R. Gemmrich, R. P. Morison, D. A. LeBel, and T. Dickey, 2012: An overview of sea state conditions and air–sea fluxes during RaDyO. *J. Geophys. Res.*, **117**, C00H19, doi:10.1029/2011JC007336.